Remote Sensing in Ecology and Conservation
Open Access
ZSL LET'S WORK FOR WILDLIFE

ORIGINAL RESEARCH

Quantifying large-scale ecosystem stability with remote sensing data

Hannah J. White[1,2], Willson Gaul[1,2], Dinara Sadykova[3], Lupe León-Sánchez[3], Paul Caplat[3,4], Mark C. Emmerson[3,4] & Jon M. Yearsley[1,2]

[1]School of Biology and Environmental Science, University College Dublin, Dublin, Ireland
[2]UCD Earth Institute, University College Dublin, Dublin, Ireland
[3]School of Biological Sciences, Queen's University Belfast, Belfast, United Kingdom
[4]Institute of Global Food Security (IGFS), Queen's University Belfast, Belfast, United Kingdom

Keywords
Ecosystem functioning, resilience, satellite, stability, vegetation index

Correspondence
Hannah J. White, School of Biology and Environmental Science, University College Dublin, Dublin, Ireland. E-mail: hannah.white@ucd.ie

Editor: Nathalie Pettorelli
Associate Editor: András Zlinszky

Received: 25 June 2019; Revised: 17 December 2019; Accepted: 17 January 2020

doi: 10.1002/rse2.148

Remote Sensing in Ecology and Conservation 2020;**6** (3):354–365

Abstract

To fully understand ecosystem functioning under global change, we need to be able to measure the stability of ecosystem functioning at multiple spatial scales. Although a number of stability components have been established at small spatial scales, there has been little progress in scaling these measures up to the landscape. Remote sensing data holds huge potential for studying processes at landscape scales but requires quantitative measures that are comparable from experimental field data to satellite remote sensing. Here we present a methodology to extract four components of ecosystem functioning stability from satellite-derived time series of Enhanced Vegetation Index (EVI) data. The four stability components are as follows: variability, resistance, recovery time and recovery rate in ecosystem functioning. We apply our method to the island of Ireland to demonstrate the use of remotely sensed data to identify large disturbance events in productivity. Our method uses stability measures that have been established at the field-plot scale to quantify the stability of ecosystem functioning. This makes our method consistent with previous small-scale stability research, whilst dealing with the unique challenges of using remotely sensed data including noise. We encourage the use of remotely-sensed data in assessing the stability of ecosystems at a scale that is relevant to conservation and management practices.

Introduction

Remotely sensed data products have revolutionized ecological studies by allowing us to investigate ecological processes which have previously only been studied at small spatial scales. Making ecosystem data comparable across spatial scale is vital if we are to fully understand ecosystem functioning under global change. The response of ecosystems to environmental disturbances can have significant ecological and economic impacts (Costanza et al. 1997; Oliver et al. 2015), yet these responses have frequently been established only at the plot level. The projected increase in extreme climatic events with ongoing climate change (Beniston et al. 2007; Mora et al. 2013) makes it imperative to better understand how systems will respond to these events at multiple spatial scales. Additional environmental pressures such as increased pollution and pest or disease outbreaks also impact ecosystem functioning (Millennium Ecosystem Assessment 2005; Seidl et al. 2016). Therefore, quantifying a system's stability in terms of its functioning is vital for predicting the effects of environmental disturbances, and remote sensing provides a unique tool to enable this.

In ecological terms, stability is a multidimensional concept which captures the capacity for ecosystems to absorb and recover from environmental disturbance in terms of their functioning (Donohue et al. 2013, 2016; Hillebrand et al. 2017). These characteristics have often been established at small spatial scales using experimental manipulations as environmental disturbances, such as small grassland plot experiments (e.g. Tilman 1996; Van Ruijven and Berendse 2010), bacterial communities in

Petri dishes (e.g. Awasthi et al. 2014) and aquatic mesocosm setups (e.g. Hillebrand et al. 2017). The stability of ecosystem functioning at large spatial scales which experience natural environmental disturbances is less well established in the literature but has recently started to be investigated (e.g. Lloret et al. 2007; Van Rooijen et al. 2015; Spasojevic et al. 2016). However, temporal monitoring of functioning over large extents is challenging, which can make upscaling relevant measures of stability difficult (Reyer et al. 2015; Van Rooijen et al. 2015), particularly when the exact timing and magnitude of environmental disturbances remain unknown.

Ecological stability is often described in terms of resistance, resilience and temporal variability (Grimm et al. 1992). These measures use a time series of an ecosystem property and calculate the deviation of this property away from its typical behaviour. Variability measures the overall temporal stability of a system and is frequently measured as either the coefficient of variation or the variance (Tilman 1996; Van Rooijen et al. 2015). Resistance reflects the capacity for a system to absorb a disturbance (Pimm 1984; Tilman and Downing 1994; Tilman 1996). Resilience (in terms of engineering resilience) quantifies the post-disturbance recovery of an ecosystem property to its equilibrium state, and is often measured as a rate (Pimm 1984; Tilman and Downing 1994; Lhermitte et al. 2011). These are shown in Figure 1. The relationship between different stability components can vary with disturbance type (Donohue et al. 2013; Arnoldi et al. 2019), highlighting the need to consider multiple measures of stability simultaneously (Donohue et al. 2016) without amalgamating them into a single measure (e.g. Holling 1973). Understanding the dynamics of multiple dimensions of stability is, therefore, crucial to ecological management and needs to be measurable in both experimental and natural systems.

Remote sensing data can provide large-scale estimates of ecosystem productivity at a relatively high temporal resolution using vegetation indices (Huete et al. 2002) such as the normalised difference vegetation index (NDVI) and the enhanced vegetation index (EVI). These capture the greenness of vegetation within an area and are a useful tool to assess primary productivity of vegetation (Pettorelli et al. 2005; Sims et al. 2006). Remotely sensed vegetation indices, therefore, allow the investigation of how ecosystem productivity responds to natural disturbances (Oehri et al. 2017) as opposed to experimental manipulations which may or may not be representative of real-world scenarios (Beier et al. 2012). They also facilitate the investigation of a host of potential disturbance types, such as wildfires or land use management (e.g. Ares et al. 2001; Goetz et al. 2006), as opposed to a single climatic event. While it is possible to investigate the stability of ecosystem functioning at large spatial

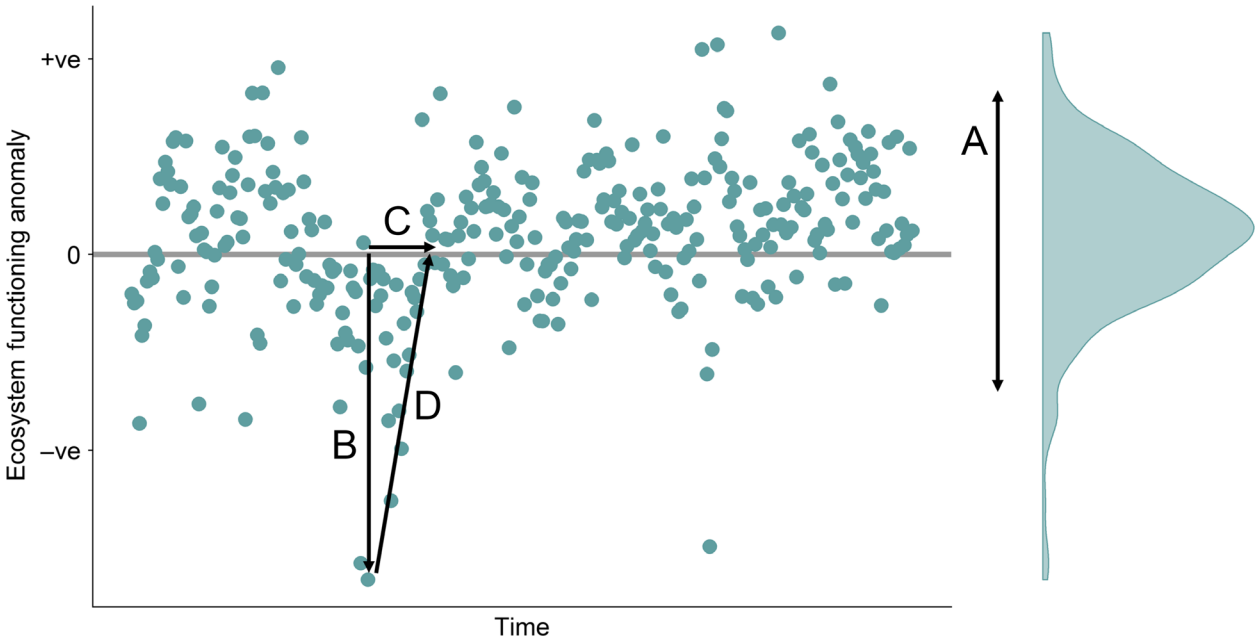

Figure 1. Common measures of ecosystem functioning stability where (A) is the overall temporal variability in ecosystem functioning, (B) is the resistance, (C) is the recovery time, and (D) is the recovery rate (defined as resistance/recovery time) which is a measure of engineering resilience. The *y* axis represents the anomaly in ecosystem functioning where +ve reflects values functioning greater than expected from that grid square in that particular month, and −ve reflects functioning lower than expected from that grid square in that particular month.

scales, significant barriers remain through the use of remotely sensed data: (1) inherent noise within the data due to atmospheric conditions, water, surface reflectance properties, or shadow (Pettorelli et al. 2005; Hird and McDermid 2009); and (2) the unknown timing of environmental disturbances from which to measure recovery time and resistance.

Various problems present themselves when scaling up different stability measures to the landscape scale. For example, the noise associated with remotely sensed data (Samanta et al. 2012; Priyadarshi et al. 2018) can obscure the exact timing and recovery of disturbance events. To account for this noise within the data, some studies that use time series of vegetation indices apply smoothing approaches, e.g. Savitsky-Gloay filter (Ali et al. 2016; Watmough et al. 2019). The performance of smoothing algorithms, however, can vary (Hird and McDermid 2009; Cai et al. 2017) and can introduce bias into data values.

Satellite-derived vegetation indices are rarely used within the literature to estimate ecosystem stability, although a handful of studies do exist, which look at recovery after known disturbance events including climatic events (Washington-Allen et al. 2008; De Keersmaecker et al. 2016) and wildfires (Goetz et al. 2006; Lhermitte et al. 2011; Spasojevic et al. 2016). In all these cases, there is a known period of pre-disturbance and post-disturbance, and also the presence of undisturbed (e.g. an unburnt control plot) areas, for comparison. The slope of the ratio of the disturbed and undisturbed vegetation indices through time post-burn, provides a metric of recovery (Spasojevic et al. 2016). However, often, we do not have a clear control with which to compare disturbed systems, particularly in the context of climatic events. Recently, stability in terms of temporal variability has been calculated using satellite-derived EVI (Mazzochini et al. 2019), however, additional stability measures related to ecosystem recovery, analogous to those established at the field scale, are still somewhat absent from the literature. Therefore, a series of stability measures that can be applied at the landscape scale, irrespective of disturbance type and location need to be developed to enable the assessment of ecosystem functioning in the light of environmental change.

There is a need for large-scale assessments of ecosystem stability to environmental disturbances, even when the precise disturbance is unknown or multifaceted. In this paper, we present a methodology to calculate a series of stability measures using remotely sensed data. We apply these measures to the island of Ireland where we have anecdotal evidence of major disturbances in productivity without underlying extreme climatic events as disturbances, e.g. the 'Fodder Crisis' of 2012-2013 (Department of Agriculture Food and the Marine 2017; Green et al. 2018).

Materials and Methods

Data

EVI data were obtained for the geographic area of the island of Ireland from the Moderate Resolution Imaging Spectrometer (MODISv6; http://modis.gsfc.nasa.gov/) for January 2003–February 2019. Sixteen-day composite images (MODIS products MYD13Q1 and MOD13Q1) were used to eliminate most of the cloud cover in daily images. Images from MODIS sensors onboard both the TERRA and AQUA satellites were downloaded so that combined we had EVI data at a temporal resolution of 8-day intervals across the entire time period. EVI captures the photosynthetic activity of an area, i.e. its 'greenness', and can be used to estimate ecosystem functioning of an area through its relationship with above-ground biomass production (Sims et al. 2006; Shi et al. 2017). It is calculated using the reflectance of three wavelengths: red (620–670 nm), near infrared (841–876 nm) and blue (459–479 nm). Other vegetation indices exist including the Normalized Difference Vegetation Index (NDVI) which uses only the red and near infrared bands. However, by incorporating the blue band into its calculation, EVI corrects for aerosol influences. In terms of the island of Ireland, which is predominantly covered by productive grasslands (>60% (Central Statistics Office, Ireland 2012)), EVI is particularly useful as it does not saturate in high biomass conditions in contrast to other vegetation indices (Huete 1988; Huete et al. 2002).

The MODIS EVI product is available at a pixel resolution of 250 × 250 m. Pixels with a reliability score less than zero (no data) or greater than one (snow, ice or cloudy) were removed. Additionally, any pixels with negative EVI values we set to have an EVI of 0 as this represents the absence of vegetation within the pixel. To avoid the influence of spurious EVI measurements on stability measures, pixels were aggregated by calculating the median at the spatial resolution of 1 × 1 km grid cells. Pixels with less than 50% land, determined from the CORINE 2012 land cover data (http://www.eea.europa.eu), were removed before calculating measures leaving 82 279 grid cells.

Like most time series data, EVI contains a seasonal component due to phenology through time, which could mask signals of resilience (De Keersmaecker et al. 2015). This, therefore, needs to be corrected for prior to calculating any temporal measures. To remove the seasonal variation in EVI, the scaled EVI anomaly was calculated

for each data point, similar to Goetz et al. (2006). The scaled EVI anomaly, $\Delta_{EVI}(i, t)$, of grid square i at date t is calculated as

$$\Delta_{EVI}(i,t) = (EVI(i,t) - \text{mean}_{u\in m}[EVI(i,u)])/\text{sd}_{u\in m}[EVI(i,u)]$$

where $EVI(i, t)$ is the EVI of grid square i at date t, m is a month of the year and $\text{mean}_{u\in m}[EVI(i, u)])$ and $\text{sd}_{u\in m}[EVI(i, u)]$ are the mean and standard deviation of EVI for grid square i over all dates, u, across the entire period (2000–2019) falling within month m, respectively. The anomaly, therefore, is unitless, but is on a scale where the interval is one standard deviation of the EVI from the grid square and the month in question. An anomaly of zero represents a baseline value of productivity.

Measures of stability

We developed four measures of EVI stability: variability, resistance, recovery time and recovery rate (engineering resilience), and applied these to EVI data from 2003 to 2019 for the island of Ireland.

When evaluating natural disturbances, as in this study, it is necessary to identify when and where these disturbances have occurred or are occurring. To identify disturbances to EVI events, we searched the time series of EVI anomalies at each grid square using the following algorithm:

1 1 Record the largest negative EVI anomaly less than −2 in the time series as well as its date, and remove this value from the time series.
2 Remove all anomalies (i.e. data points) which fall within 180 days each side of the recorded anomaly. This time threshold of 180 days was selected by estimating the distribution of return times (see below for return time calculation) and determining the return time for which it took 97.5% anomalies to return to an anomaly of zero (i.e. the baseline).
3 Return to step 1 if an anomaly less than −2 is still present in the time series, otherwise stop.

This algorithm gave a set of dates, $\boldsymbol{T}$, and magnitudes, $\boldsymbol{M}$, of independent EVI anomalies falling at least two standard deviations below the zero baseline. The pair $\{T_j, M_j\}$ together is called a two-sigma event, and we represent this as $\{T_j, M_j\}_i$ for the jth disturbance in grid square i. The choice of a two standard deviation threshold is arbitrary, and other thresholds can be used. For example, one-sigma events, which are independent EVI anomalies falling at least one standard deviation below the zero baseline, could be calculated but would represent less extreme anomalies in functioning.

Resistance

Resistance is a measure of the capacity for a system to absorb an environmental disturbance and is usually calculated as the immediate change or drop in functioning following the disturbance event (Pimm 1984; Tilman and Downing 1994). Resistance for grid square i was calculated as the reciprocal of the absolute value of the two-sigma event magnitudes (Resistance = $1/|(M_j)_i|$). From all these resistances for grid square i, we calculated the smallest resistance and the mean resistance. Defining resistance using the reciprocal of two-sigma event magnitudes makes the interpretation of the resistance more intuitive (higher resistance represents a smaller deviation from the baseline).

Recovery time

In field experiments, the recovery of ecosystem functioning following a disturbance is often measured by the ratio of control to disturbed biomass at some time following the disturbance (Van Ruijven and Berendse 2010; Mariotte et al. 2013; Xu et al. 2014). However, this experimental measure of recovery is a poor estimate of recovery time because only a couple of time-points post-disturbance are logistically feasible.

The use of long-term time series of vegetation indices from remote sensing data provides an opportunity to estimate a recovery time that more strictly fits the definition of engineering resilience as a measure of return to equilibrium after a disturbance (Pimm 1984). However, remote sensing data also poses challenges in terms of timing of disturbance events from which to measure the recovery and substantial noise within the data, which masks some of the recovery dynamics. To solve these challenges, the time and magnitude of two-sigma events using our algorithm $\{T_j, M_j\}_i$ were defined and then a temporal moving window algorithm was used to reduce the effect of noise inducing factors, such as clouds or aerosol levels, by calculating the average EVI anomaly within the window:

$$W(i,t) = \sum_{\tau=0}^{5} \Delta_{EVI}(i, t + 8\tau)/6,$$

where τ indexes the number of MODIS data points. The moving window spanned 48 days (six MODIS time points). Window sizes from three to fifteen MODIS time points were examined and over a window size of six MODIS time points appeared to have little effect on average anomaly (Fig. S1). Using a moving window algorithm on the EVI anomaly provides an alternative approach to smoothing filters which can obscure important signals

within the data, but similarly deals with noise from poor atmospheric conditions which can have a larger effect on stability estimates than temporal resolution (De Keersmaecker et al. 2014).

The recovery time, T_{ji}, was calculated for the j^{th} two-sigma event in grid square i as the minimum time taken for the moving window average, $W(i,t)$, to become non-negative:

$$T_{ji} = \min\left[t - T_{ji} | W(i,t) \geq 0 \,\&\, t > T_{ji}\right],$$

where T_{ji} is the time of the j^{th} two-sigma event in grid square i and t is time after this event. For each site, a single value for return time was produced by selecting all two-sigma events (i.e. $M_{ji}<-2$ for all j) and calculating the mean within each grid cell.

Recovery rate

The rate of recovery of the j^{th} disturbance in grid square i was calculated as $R_{ji} = M_{ji}/T_{ji}$, where high values of R represent fast rates of recovery. As with the previous measures, a single value of recovery rate for each grid square was taken as the mean recovery rate from all two-sigma events (i.e. $M_{ji}<-2$ for all j). Including rate of recovery in addition to recovery time is important as it accounts for the magnitude of the anomaly.

Variability

Temporal variability in the unscaled EVI anomaly at grid square i (v_i) represents the instability in productivity in a system across an entire time period. In the present case, this was calculated for the time period 2003–2019.

$$v_i = \mathrm{sd}[\mathrm{EVI}(i,t) - \mathrm{mean}_{u \in m}[\mathrm{EVI}(i,u)]]^2,$$

where $\mathrm{mean}_{u \in m}$ [EVI(i, u)] is the mean of EVI for grid square i over all dates, u, across the entire period (2000–2019) falling within month m and sd is the standard deviation across all time points, t.

Timing of events

The dates of the disturbance to EVI (T_j) with the longest (maximum) recovery time and slowest (minimum) recovery rates in each site were calculated. These represent the largest disturbance events to productivity.

Analyses

The relationships between the aggregated measures of stability for a grid square (variability, mean resistance, mean recovery time, mean recovery rate, longest recovery time, and slowest recovery rate) were estimated using Spearman's rank correlations, which allow for non-linear, monotonic correlations using the *rcorr* function in the R package Hmisc (Harrell Jnr 2018). The spatial autocorrelation of all the measures was calculated with Moran's I using the *moran* function in the R package spdep (Bivand et al. 2013; Bivand and Piras 2015). The timing of the two-sigma events as well as those with the largest anomalies, longest recovery times and slowest recovery rates, were plotted. The trend in the frequency of events over time was estimated using all two-sigma events. These two-sigma events were pooled by year and their count fitted using a generalised linear model (GLM) with a negative binomial error distribution and log link function with number of events as the dependent variable, and year as a quantitative independent variable using the *glm.nb* function in the R package MASS (Venables and Ripley 2002). All data processing and analyses were carried out in Rv3.5.1 (R Core Team 2018). R code is available at the GitHub repository https://github.com/HannahWhite/StabilityMetrics.

Results

Over the 16-year time period studied, nearly all 1 × 1 km grid cells in Ireland (99.8% of the 82279 squares) experienced at least one-two-sigma events (an event which fell more than two standard deviations below the baseline). The number of two-sigma events in each grid cell ranged from 0 to 21. All stability measures showed spatial variation across the island of Ireland (Fig. 2) and Moran's I (a measure of spatial autocorrelation, Moran (1950)) reached zero at less than 50 km for all the stability measures (Fig. S2).

All correlations between the stability measures were significant at the 5% level (Fig. 3). The strongest correlation was between recovery time and recovery rate ($R = -0.62$, $P < 0.001$).

Visual inspection shows no clear clusters of peaks in the time for the occurrence of two-sigma events (Fig. 4A and B). However, clear peaks in the numbers of events over time occurred for two stability measures: the longest recovery time and slowest recovery rate within a square (for example late 2009 and throughout 2012; Fig. 4C and D). We found no evidence that two-sigma events have become more common over time (linear term coefficient from a negative binomial GLM = 0.0038, standard error = 0.0034, df = 14, $P = 0.26$; Fig. 5).

Discussion

We present an approach that takes the definitions of resistance, resilience, and variability which have been

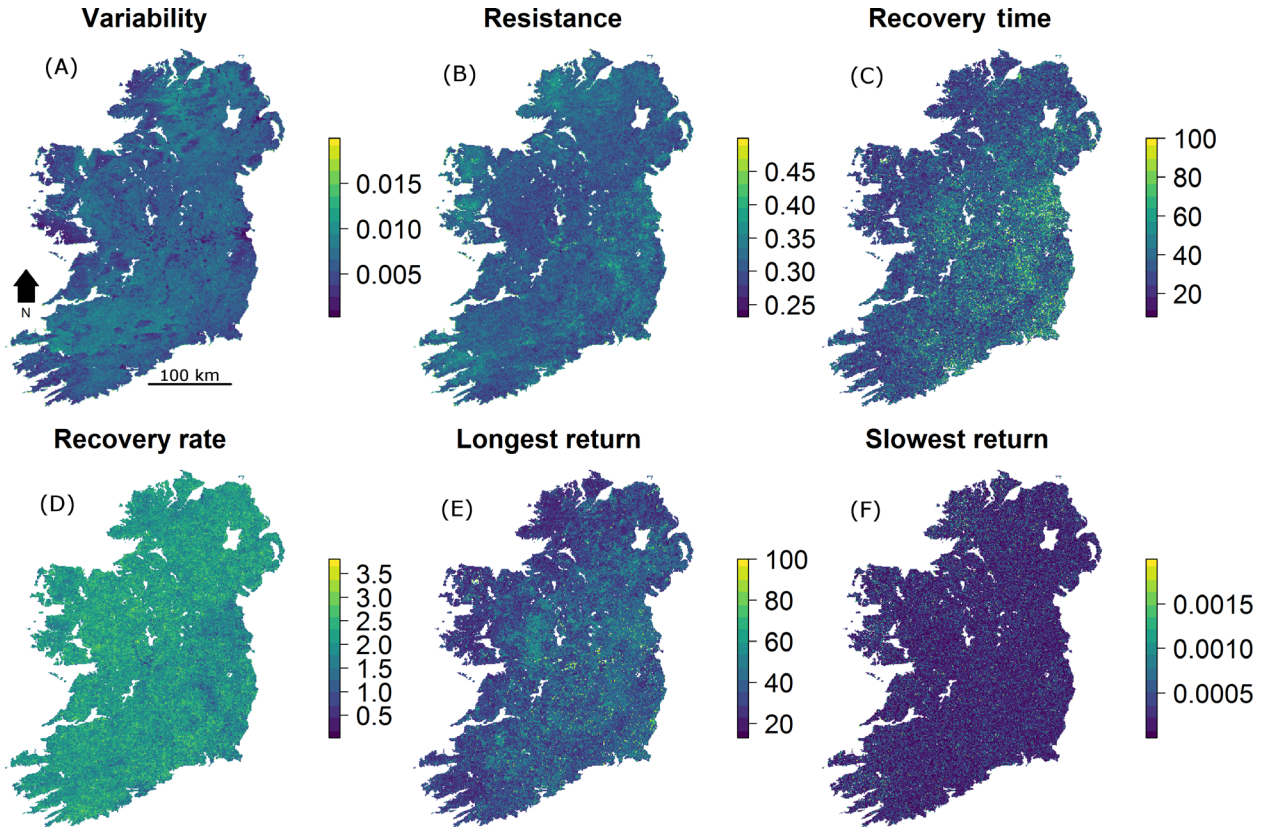

Figure 2. Maps showing spatial variation of our EVI stability measure at a spatial resolution of 1 × 1 km. (A) temporal variation in the unscaled EVI anomaly, (B) mean magnitude of two-sigma events, (C) mean recovery time from two-sigma events (days), (D) mean recovery rate from two-sigma events, (E) the longest recovery time back to zero from a negative EVI anomaly (days), and (F) the slowest recovery rate.

measured at the field plot scale using biomass samples (e.g. Tilman and Downing 1994; Van Ruijven and Berendse 2010), and scales them up using satellite-derived EVI data, while dealing with specific properties inherent to this type of data. Being able to measure ecosystem stability is crucial to understanding the impacts of ongoing global change. Managing for ecosystem stability has been called for by a number of international bodies including the Intergovernmental Science-Policy Platform on Biodiversity and Ecosystem Services (IPBES; Díaz et al. 2015), and is linked to multiple United Nations Sustainable Development Goals (https://sustainabledevelopment.un.org/). The scale at which environmental impacts on ecosystems are measured, however, is vital, particularly in the context of adaptive management (Reidsma et al. 2010). Models derived from small-scale ecological data are unlikely to predict large-scale impacts of anthropogenic pressures (Kerr and Ostrovsky 2003). Developing measures to assess landscape-scale stability of vegetation is important as this scale is relevant to management and conservation practices to maintain the functioning of ecosystems from which we derive a range of goods and services (Suding 2011; Spasojevic et al. 2016; Mori et al. 2018). The availability of satellite-derived vegetation indices has facilitated increased efforts for assessment of ecosystem stability through cost-effective evaluation of landscapes and their characteristics (Kerr and Ostrovsky 2003; Neigh et al. 2008). However, existing stability measures using remotely sensed data do not match the stability measures frequently used at the field scale (e.g. Ares et al. 2001; De Keersmaecker et al. 2015).

The approach presented here differs from the handful of remote sensing approaches that measure stability with respect to a particular environmental disturbance e.g. climate anomalies (Washington-Allen et al. 2008; Keersmaecker et al. 2016), fire disturbance (Goetz et al. 2006; Spasojevic et al. 2016; Yang et al. 2017) and human land use change (Ares et al. 2001). Here, ecosystem functioning data itself (EVI, reflecting primary production) is used to identify disturbances to ecosystem functioning measured using the EVI anomaly, irrespective of data on the physical environment. Frequently within the ecological stability literature, the effect of known environmental disturbance events is the main focus (Donohue et al.

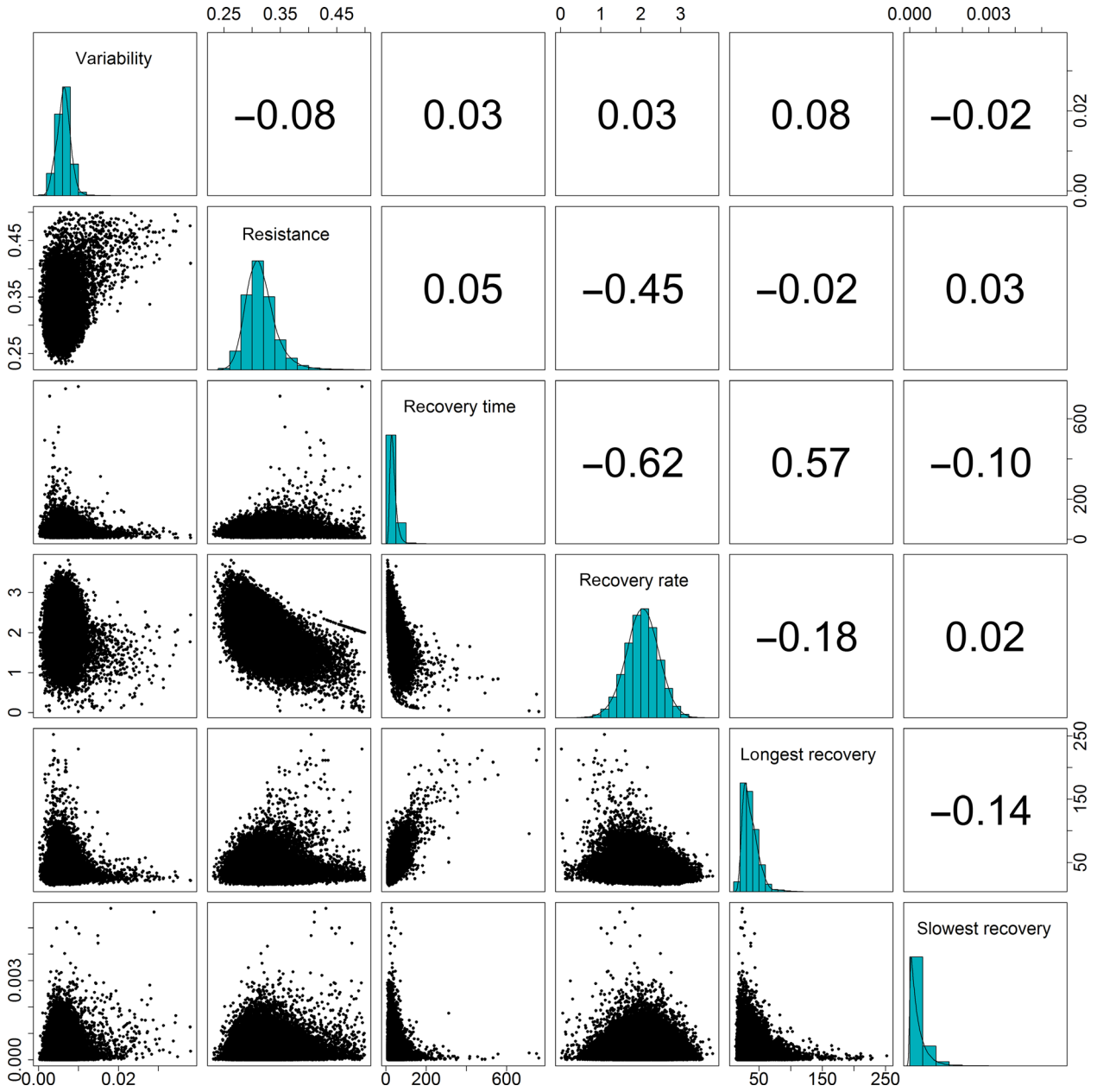

Figure 3. Correlations (Spearman's rho) between temporal variation in the unscaled EVI anomaly, mean magnitude of two-sigma events, mean recovery time from two-sigma events, mean recovery rate from two-sigma events, the longest recovery time back to zero from a negative EVI anomaly, and the slowest recovery rate at the 1 × 1 km scale. All correlations were significant using the threshold of $P < 0.05$.

2016), however, by using data on productivity it is possible to identify disturbances to functioning and its recovery, regardless of whether a known environmental disturbance event occurred or not. Disturbances to normal ecosystem functioning such as productivity may not always be the result of a single, extreme event and the current method allows the investigation of both long-term disturbances and those that result from the cumulative impact of a combination of small environmental pressures e.g. the fodder crisis in Ireland in 2012–2013 (Green et al. 2018).

The application of this technique to the island of Ireland illustrates that the majority of disturbances to EVI with the longest recovery times fall throughout 2012 (Fig. 4C), when the fodder crisis occurred. This period also shows a peak in the number of anomalies with the

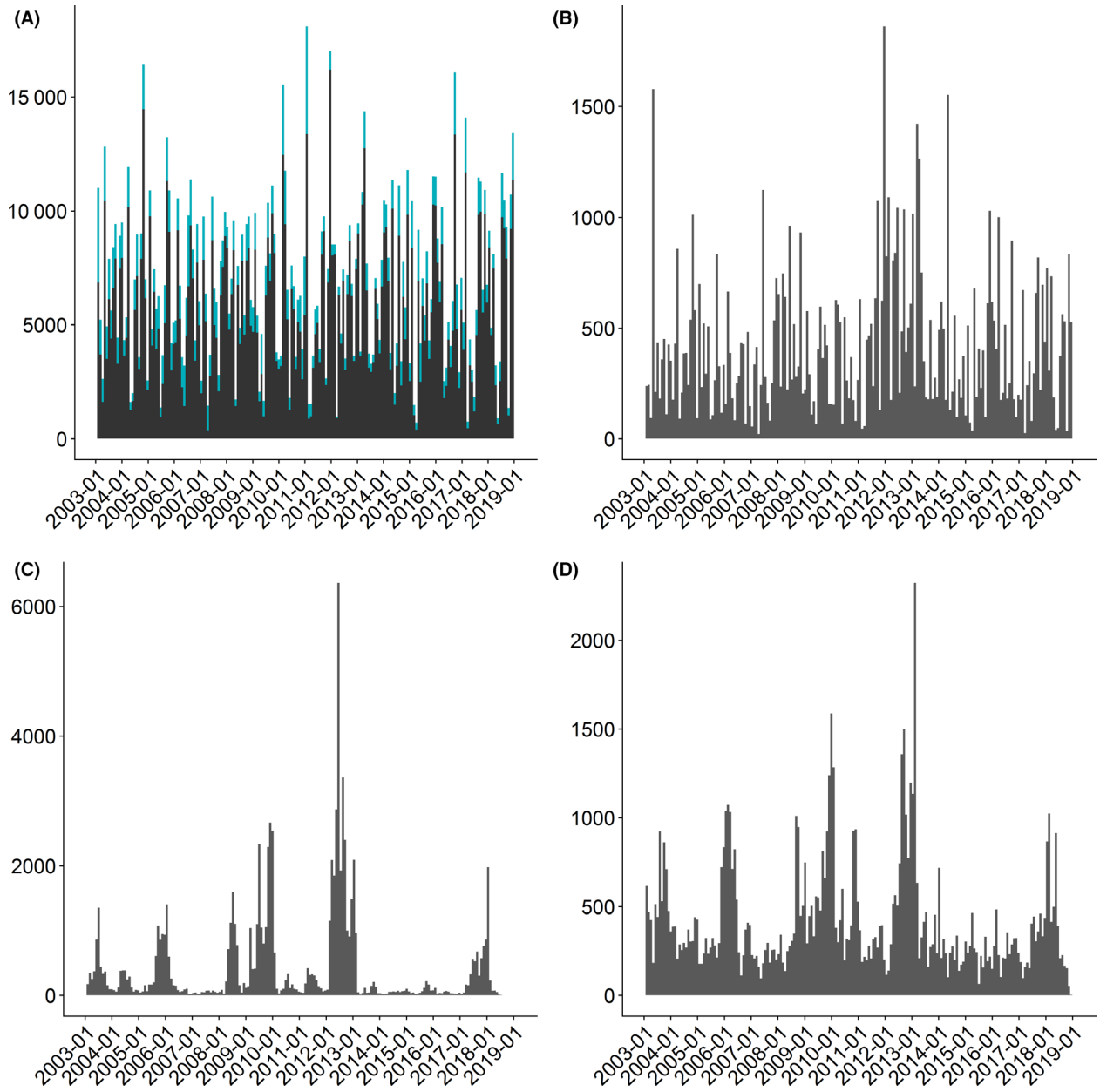

Figure 4. Counts of disturbance events at the 1 × 1 km resolution in each month showing (A) all two-sigma events (where the EVI anomaly falls more than two standard deviations below the baseline) in dark grey and one-sigma events in cyan, (B) the largest anomaly within each 1 × 1 km square, (C) the anomaly with the longest recovery time and (D) the anomaly with the slowest recovery rate within each 1 × 1 km square.

slowest recovery rates. The 2012–2013 fodder crisis is believed to have been a result of the combination of a poor growing season in 2012 followed by a long winter period (DAFM 2017). As the island of Ireland has over 50% of its land cover dedicated to improved agricultural grassland, primarily pasture (Green et al. 2018), the signal from this productive land class is clearly detectable within the results. This would explain the observation that very long recovery times followed disturbances in 2012 as the regional climatic conditions were such that productivity was unable to recover rapidly to baseline functioning. As the fodder crisis was not the result of a single extreme climatic event, this result clearly demonstrates that a disturbance in functioning can result from a combination of environmental factors, and, therefore, may not be detected by methods that rely on data describing extreme environmental or climatic events. Yet, the large repercussions for the Irish economy following the fodder crisis

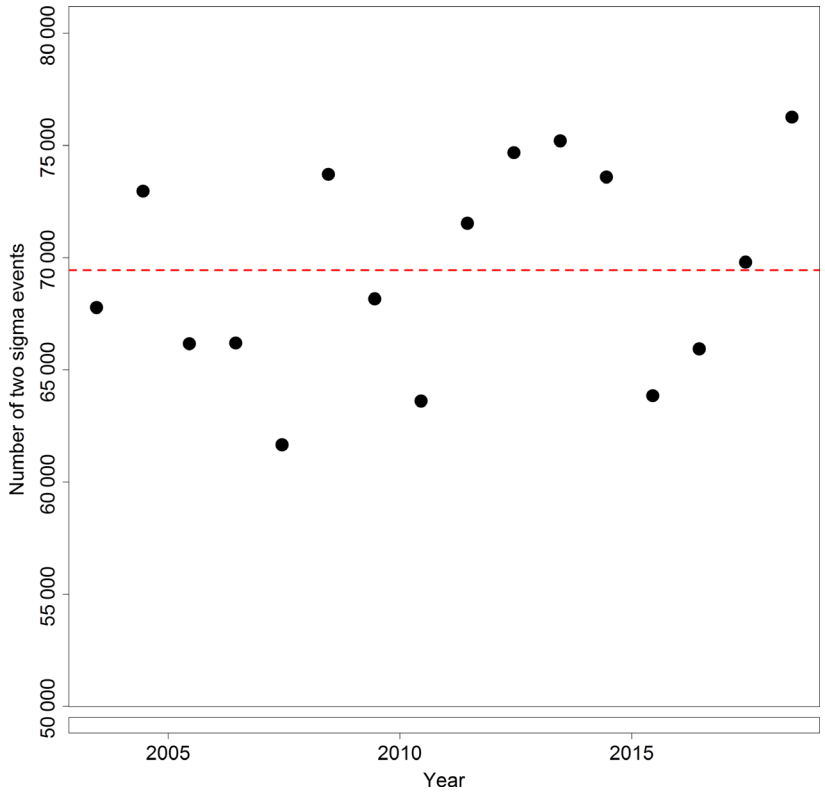

Figure 5. The number of two-sigma events (anomalies which fall more than two standard deviations below the baseline) in each year across all 1 × 1 km squares. The dashed line shows the intercept of the null model.

(Department of Agriculture Food and the Marine 2017), demonstrates the need for large scale assessments of ecosystem stability and resilience to environmental disturbances, even when the precise disturbance is unknown or multifaceted.

Other peaks in the timing of events with long recovery times and slow recovery rates correspond with known major weather events identified by Met Éireann (https://www.met.i.e/climate/major-weather-events), for example, the coldest winter in nearly 50 years in 2009/2010 (Met Éireann 2017) and the extremely wet summer of 2008 (Lennon and Walsh 2008). The additional cluster in the largest anomalies within each square that occurred towards the end of 2015 and the beginning of 2016 (Fig. 4B), however, was not captured by the measure of long or slow recoveries. Met Éireann do not have records of a major weather event during this period (https://www.met.i.e/climate/major-weather-events). It is, therefore, likely that these events represent noise within the data resulting from clouds or poor atmospheric conditions (Pettorelli et al. 2005; Priyadarshi et al. 2018), and, demonstrates the necessity to focus not just on the largest disturbance to ecosystem functioning within an area for studies of resistance. This also supports the approach presented here of taking the mean drop in productivity of all two-sigma events so that errors and biases within the data do not obscure the overall signal.

The overall number of two-sigma events per year does not appear to have changed between 2003 and 2018. Although, as noted above, some of these events are likely to be noise within the EVI data, if it is assumed that noise levels do not vary through time, then either the projected increase in frequency of extreme climatic events (Beniston et al. 2007; Mora et al. 2013) does not appear to have occurred within this relatively short time-frame, or the ecosystem has adapted to these events thus showing no increase in response signal. Applying our measures to climatic data alongside EVI data would help determine this.

The strongest correlation between our stability measures was between the mean recovery time and the mean recovery rate (this was also true at the 10 × 10 km scale Fig. S3), but generally, stability measures were only weakly correlated. This demonstrates the multidimensionality of ecosystem stability but does not match the non-independence of community stability measures outlined by Donohue et al. (2013, 2016). Further investigation under a multidimensional framework is needed to

determine the interrelationships of our stability measures through time and under different environmental conditions to determine how the relationships vary under different levels of stress (Donohue et al. 2013).

Using EVI enables the determination of stability of ecosystem functioning in terms of an area's productivity. The approach presented here, however, can be applied to any dynamic measure of an ecosystem process or function where time series data is available (Pettorelli et al. 2018), e.g. gas regulation (Spichtinger et al. 2001) or climate regulation (Jin and Dickinson 2010), as long as the temporal resolution of measurements is smaller than the length of time it takes a system to recover from a disturbance.

Conclusion

Developing methods consistent with ecological theory allow large-scale evaluation of multiple components of stability across land covers which match those that have been established using empirically collected field plot data. The timing of disturbance events with long recovery periods and slow recovery rates match anecdotal evidence, supporting the proposed method as a means to identify periods of disturbances to ecosystem functioning. Understanding stability of ecosystems at large spatial scales is crucial if we are to fully comprehend the impacts of global change and how best to manage large areas to maintain ecosystem functioning.

Acknowledgments

This publication has emanated from research conducted with the financial support of Science Foundation Ireland and the Department for the Economy, Northern Ireland under Grant number (15/IA/2881).

Data Accessibility

EVI data is available for download from http://modis.gsfc.nasa.gov/.

References

Ali, I., F. Cawkwell, E. Dwyer, and S. Green. 2016. Modeling managed grassland biomass estimation by using multitemporal remote sensing data—a machine learning approach. *IEEE J. Sel. Top. Appl. Earth Obs. Remote Sens.* **10**, 3254–3264.

Ares, J., M. Bertiller, and H. del Valle. 2001. Functional and structural landscape indicators of intensification, resilience and resistance in agroecosystems in southern Argentina based on remotely sensed data. *Landscape Ecol.* **16**, 221–234. https://doi.org/10.1023/A:1011172006029.

Arnoldi, J., M. Loreau, and B. Haegeman. 2019. The inherent multidimensionality of temporal variability: how common and rare species shape stability patterns. *Ecol. Lett.* **22**, 1557–1567. https://doi.org/10.1111/ele.13345.

Awasthi, A., M. Singh, S. K. Soni, R. Singh, and A. Kalra. 2014. Biodiversity acts as insurance of productivity of bacterial communities under abiotic perturbations. *ISME J.* **8**, 2445–2452. https://doi.org/10.1038/ismej.2014.91.

Beier, C., C. Beierkuhnlein, T. Wohlgemuth, J. Penuelas, B. Emmett, C. Körner, et al. 2012. Precipitation manipulation experiments - challenges and recommendations for the future. *Ecol. Lett.* **15**, 899–911. https://doi.org/10.1111/j.1461-0248.2012.01793.x.

Beniston, M., D. B. Stephenson, O. B. Christensen, C. A. T. Ferro, C. Frei, S. Goyette, et al. 2007. Future extreme events in European climate: an exploration of regional climate model projections. *Clim. Change.* **81**(S1), 71–95.

Bivand, R. S., and G. Piras. 2015. Comparing implementations of estimation methods for spatial econometrics. *J. Stat. Softw.* **63**, 1–36. http://www.jstatsoft.org/v63/i18

Bivand, R. S., J. Hauke, and T. Kossowski. 2013. Computing the Jacobian in Gaussian spatial autoregressive models: an illustrated comparison of available methods. *Geogr. Anal.* **45**, 150–179.

Cai, Z., P. Jönsson, H. Jin, and L. Eklundh. 2017. Performance of smoothing methods for reconstructing NDVI time-series and estimating vegetation phenology from MODIS data. *Remote Sens.* **9**, 1271.

Central Statistics Office, Ireland. 2012. *Census of agriculture 2010 - final results*. The Stationery Office, Dublin.

Costanza, R., R. D'Arge, and R. de Groot. 1997. The value of the world's ecosystem services and natural capital. *Nature* **387**, 253–260. https://doi.org/10.1038/387253a0.

De Keersmaecker, W., S. Lhermitte, O. Honnay, J. Farifteh, B. Somers, and P. Coppin. 2014. How to measure ecosystem stability? An evaluation of the reliability of stability metrics based on remote sensing time series across the major global ecosystems. *Glob. Change Biol.* **20**, 2149–2161. https://doi.org/10.1111/gcb.12495.

De Keersmaecker, W., S. Lhermitte, L. Tits, O. Honnay, B. Somers, and P. Coppin. 2015. A model quantifying global vegetation resistance and resilience to short-term climate anomalies and their relationship with vegetation cover. *Glob. Ecol. Biogeogr.* **24**, 539–548. https://doi.org/10.1111/geb.12279.

De Keersmaecker, W., N. van Rooijen, S. Lhermitte, L. Tits, J. Schaminée, P. Coppin, et al. 2016. Species-rich semi-natural grasslands have a higher resistance but a lower resilience than intensively managed agricultural grasslands in response to climate anomalies. *J. Appl. Ecol.* **53**, 430–439. https://doi.org/10.1111/1365-2664.12595.

Department of Agriculture Food and the Marine. 2017. Adaptation planning - developing resilience to climate change in the Irish agriculture and forest sector.

Díaz, S., S. Demissew, J. Carabias, C. Joly, M. Lonsdale, N. Ash, et al. 2015. The IPBES Conceptual Framework — connecting nature and people. *Curr. Opin. Environ. Sustain.* **14**, 1–16. https://doi.org/10.1016/j.cosust.2014.11.002.

Donohue, I., O. L. Petchey, J. M. Montoya, A. L. Jackson, L. McNally, M. Viana, et al. 2013. On the dimensionality of ecological stability. *Ecol. Lett.* **16**, 421–429. https://doi.org/10.1111/ele.12086.

Donohue, I., H. Hillebrand, J. M. Montoya, O. L. Petchey, S. L. Pimm, M. S. Fowler, et al. 2016. Navigating the complexity of ecological stability. *Ecol. Lett.* **19**, 1172–1185. https://doi.org/10.1111/ele.12648.

Goetz, S. J., G. J. Fiske, and A. G. Bunn. 2006. Using satellite time-series data sets to analyze fire disturbance and forest recovery across Canada. *Remote Sens. Environ.* **101**, 352–365. https://doi.org/10.1016/j.rse.2006.01.011.

Green, S., F. Cawkwell, and E. Dwyer. 2018. A time-domain NDVI anomaly service for intensively managed grassland agriculture. *Remote Sens. Appl. Soc. Environ.* **11**, 282–290.

Grimm, V., E. Schmidt, and C. Wissel. 1992. On the application of stability concepts in ecology. *Ecol. Model.* **63**, 143–161. https://doi.org/10.1016/0304-3800(92)90067-O.

Harrell Jnr, F. E.; with contributions from Charles Dupont and many others. (2018). Hmisc: Harrell Miscellaneous. R package version 4.1-1. https://CRAN.R-project.org/package=Hmisc

Hillebrand, H., S. Langenheder, K. Lebret, E. Lindström, Ö. Östman, and M. Striebel. 2017. Decomposing multiple dimensions of stability in global change experiments. *Ecol. Lett.* **21**, 21–30. https://doi.org/10.1111/ele.12867.

Hird, J. N., and G. J. McDermid. 2009. Noise reduction of NDVI time series: an empirical comparison of selected techniques. *Remote Sens. Environ.* **113**, 248–258. https://doi.org/10.1016/j.rse.2008.09.003.

Holling, C. S. 1973. Resilience and stability of ecological systems. *Annu. Rev. Ecol. Syst.* **4**, 1–23. https://doi.org/10.1146/annurev.es.04.110173.000245.

Huete, A. 1988. A soil-adjusted vegetation index (SAVI). *Remote Sens. Environ.* **25**, 295–309.

Huete, A., K. Didan, T. Miura, E. Rodriguez, X. Gao, and L. Ferreira. 2002. Overview of the radiometric and biophysical performance of the MODIS vegetation indices. *Remote Sens. Environ.* **83**, 195–213 Retrieved fromhttp://www.sciencedirect.com/science/article/pii/S0034425702000962.

Jin, M., and R. E. Dickinson. 2010. Land surface skin temperature climatology: benefitting from the strengths of satellite observations. *Environ. Res. Lett.* **5**, 044004. https://doi.org/10.1088/1748-9326/5/4/044004.

Kerr, J. T., and M. Ostrovsky. 2003. From space to species: ecological applications for remote sensing. *Trends Ecol. Evol.* **18**, 299–305. https://doi.org/10.1016/S0169-5347(03)00071-5.

Lennon, P., and S. Walsh 2008. 2008 Summer rainfall in Ireland (Vol. 2).

Lhermitte, S., J. Verbesselt, W. W. Verstraeten, S. Veraverbeke, and P. Coppin. 2011. Assessing intra-annual vegetation regrowth after fire using the pixel based regeneration index. *ISPRS J. Photogramm. Remote Sens.* **66**, 17–27.

Lloret, A. F., A. Lobo, H. Estevan, P. Maisongrande, J. Vayreda, and J. Terradas. 2007. Woody plant richness and NDVI response to drought events in Catalonian (Northeastern Spain) forests. *Ecology* **88**, 2270–2279.

Mariotte, P., C. Vandenberghe, P. Kardol, F. Hagedorn, and A. Buttler. 2013. Subordinate plant species enhance community resistance against drought in semi-natural grasslands. *J. Ecol.* **101**, 763–773.

Mazzochini, G. G., C. R. Fonseca, G. C. Costa, R. M. Santos, A. T. Oliveira-Filho, and G. Ganade. 2019. Plant phylogenetic diversity stabilizes large-scale ecosystem productivity. *Glob. Ecol. Biogeogr.* **28**, 1430–1439. https://doi.org/10.1111/geb.12963.

Met Éireann. 2017. Exceptional weather events: cold weather Winter 2009/10. https://www.met.ie/cms/assets/uploads/2017/08/Winter2009-10.pdf

Millennium Ecosystem Assessment. 2005. *Ecosystems and human well-being: synthesis*. Island Press, Washington DC.

Mora, C., A. G. Frazier, R. J. Longman, R. S. Dacks, M. M. Walton, E. J. Tong, et al. 2013. The projected timing of climate departure from recent variability. *Nature* **502**, 183–187.

Moran, A. P. A. P. 1950. Notes on continuous stochastic phenomena. *Biometrika* **37**, 17–23 https://doi.org/137.43.85.230

Mori, A. S., F. Isbell, and R. Seidl. 2018. β-diversity, community assembly, and ecosystem functioning. *Trends Ecol. Evol.* **33**, 549–564. https://doi.org/10.1016/j.tree.2018.04.012.

Neigh, C. S. R., C. J. Tucker, and J. R. G. Townshend. 2008. North American vegetation dynamics observed with multi-resolution satellite data. *Remote Sens. Environ.* **112**, 1749–1772. https://doi.org/10.1016/j.rse.2007.08.018.

Oehri, J., B. Schmid, G. Schaepman-Strub, and P. A. Niklaus. 2017. Biodiversity promotes primary productivity and growing season lengthening at the landscape scale. *Proc. Natl. Acad. Sci. USA* **114**, 10160–10165.

Oliver, T. H., M. S. Heard, N. J. B. Isaac, D. B. Roy, D. Procter, F. Eigenbrod, et al. 2015. Biodiversity and resilience of ecosystem functions. *Trends Ecol. Evol.* **30**, 673–684.

Pettorelli, N., H. Schulte to Bühne, A. Tulloch, G. Dubois, C. Macinnis-Ng, A. M. Queirós, et al. 2018. Satellite remote sensing of ecosystem functions: opportunities, challenges and way forward. *Remote Sens. Ecol. Conserv.* **4**, 71–93.

Pettorelli, N., J. O. Vik, A. Mysterud, J. M. Gaillard, C. J. Tucker, and N. C. Stenseth. 2005. Using the satellite-derived NDVI to assess ecological responses to environmental change. *Trends Ecol. Evol.* https://doi.org/10.1016/j.tree.2005.05.011.

Pimm, S. L. 1984. The complexity and stability of ecosystems. *Nature* **307**, 321–326.

Priyadarshi, N., V. M. Chowdary, Y. K. Srivastava, I. C. Das, and C. S. Jha. 2018. Reconstruction of time series MODIS EVI data using de-noising algorithms. *Geocarto Int.* **33**, 1095–1113. https://doi.org/10.1080/10106049.2017.1333535.

R Core Team. 2018. *R a language and environment for statistical computing*. R Foundation for Statistical Computing, Vienna, Austria https://www.R-project.org.

Reidsma, P., F. Ewert, A. O. Lansink, and R. Leemans. 2010. Adaptation to climate change and climate variability in European agriculture: the importance of farm level responses. *Eur. J. Agron.* **32**, 91–102.

Reyer, C. P. O., N. Brouwers, A. Rammig, B. W. Brook, J. Epila, R. F. Grant, et al. 2015. Forest resilience and tipping points at different spatio-temporal scales: approaches and challenges. *J. Ecol.* **103**, 5–15. https://doi.org/10.1111/1365-2745.12337.

Samanta, A., S. Ganguly, E. Vermote, R. R. Nemani, and R. B. Myneni. 2012. Why is remote sensing of Amazon forest greenness so challenging? *Earth Interact.* **16**, 1–14. https://doi.org/10.1175/2012EI440.1.

Seidl, R., T. A. Spies, D. L. Peterson, S. L. Stephens, and J. A. Hicke. 2016. Searching for resilience: addressing the impacts of changing disturbance regimes on forest ecosystem services. *J. Appl. Ecol.* **53**, 120–129.

Shi, H., L. Li, D. Eamus, A. Huete, J. Cleverly, X. Tian, et al. 2017. Assessing the ability of MODIS EVI to estimate terrestrial ecosystem gross primary production of multiple land cover types. *Ecol. Ind.* **72**, 153–164. https://doi.org/10.1016/j.ecolind.2016.08.022.

Sims, D. A., A. F. Rahman, V. D. Cordova, B. Z. El-Masri, D. D. Baldocchi, L. B. Flanagan, et al. 2006. On the use of MODIS EVI to assess gross primary productivity of North American ecosystems. *J. Geophys. Res. Biogeosci.* **111**, 1–16. https://doi.org/10.1029/2006JG000162.

Spasojevic, M. J., C. A. Bahlai, B. A. Bradley, B. J. Butterfield, M. Tuanmu, S. Sistla, et al. 2016. Scaling up the diversity-resilience relationship with trait databases and remote sensing data: the recovery of productivity after wildfire. *Glob. Change Biol.* **22**, 1421–1432.

Spichtinger, N., M. Wenig, P. James, T. Wagner, U. Platt, and A. Stohl. 2001. Satellite detection of a continental-scale plume of nitrogen oxides from boreal forest fires. *Geophys. Res. Lett.* **28**, 4579–4582.

Suding, K. N. 2011. Toward an era of restoration in ecology: successes, failures, and opportunities ahead. *Annu. Rev. Ecol. Evol. Syst.* **42**, 465–487. https://doi.org/10.1146/annurev-ecolsys-102710-145115.

Tilman, D. 1996. Biodiversity: population versus ecosystem stability. *Ecology* **77**, 350–363.

Tilman, D., and J. A. Downing. 1994. Biodiversity and stability in grasslands. *Nature* **367**, 363–365.

Van Rooijen, N. M., W. de Keersmaecker, W. A. Ozinga, P. Coppin, S. M. Hennekens, J. H. J. Schaminée, et al. 2015. Plant species diversity mediates ecosystem stability of natural dune grasslands in response to drought. *Ecosystems* **18**, 1383–1394. https://doi.org/10.1007/s10021-015-9905-6.

Van Ruijven, J., and F. Berendse. 2010. Diversity enhances community recovery, but not resistance, after drought. *J. Ecol.* **98**, 81–86. https://doi.org/10.1111/j.1365-2745.2009.01603.x.

Venables, W. N., and B. D. Ripley. 2002. *Modern applied statistics with S*, 4th ed.. Springer, New York.

Washington-Allen, R. A., R. D. Ramsey, N. E. West, and B. E. Norton. 2008. Quantification of the ecological resilience of drylands using digital remote sensing. *Ecol. Soc.* **13**, 33.

Watmough, G. R., C. L. J. Marcinko, C. Sullivan, K. Tschirhart, P. K. Mutuo, C. A. Palm, et al. 2019. Socioecologically informed use of remote sensing data to predict rural household poverty. *Proc. Natl. Acad. Sci.* **116**, 201812969. https://doi.org/10.1073/pnas.1812969116.

Xu, Z., H. Ren, J. Cai, R. Wang, M. H. Li, S. Wan, et al. 2014. Effects of experimentally-enhanced precipitation and nitrogen on resistance, recovery and resilience of a semi-arid grassland after drought. *Oecologia* **176**, 1187–1197.

Yang, J., S. Pan, S. Dangal, B. Zhang, S. Wang, and H. Tian. 2017. Continental-scale quantification of post-fire vegetation greenness recovery in temperate and boreal North America. *Remote Sens. Environ.* **199**, 277–290.

Supporting Information

Additional supporting information may be found online in the Supporting Information section at the end of the article.

Figure S1. Plot of average EVI anomaly within moving window for various moving window sizes for 10 randomly selected grid squares shown in different colours starting at the 60th time point of the time series of EVI anomalies (selected randomly).

Figure S2. Correlogram of Moran's I measure of spatial autocorrelation with distance in kilometers for the six measures of stability at the 1 × 1 km spatial scale.

Figure S3. Correlations (Spearman's rho) between six measures of stability measured at the 10 × 10 km scale. * indicate correlations where $P < 0.05$.

